Chemistry & Biology, Vol. 10, 175–187, February, 2003, ©2003 Elsevier Science Ltd. All rights reserved. DOI 10.1016/S1074-5521(03)00024-3

Encapsulating Streptomycin within a Small 40-mer RNA

Valentina Tereshko,[1] Eugene Skripkin,[1] and Dinshaw J. Patel*
Cellular Biochemistry & Biophysics Program
Memorial Sloan-Kettering Cancer Center
New York, New York 10021

Summary

We describe a 2.9 Å X-ray structure of a complex between the aminocyclitol antibiotic streptomycin and an in vitro selected RNA aptamer, solved using the anomalous diffraction properties of Ba cations. The RNA aptamer, which contains two asymmetric internal loops, adopts a distinct cation-stabilized fold involving a series of S-shaped backbone turns anchored by canonical and noncanonical pairs and triples. The streptomycin streptose ring is encapsulated by stacked arrays of bases from both loops at the elbow of the L-shaped RNA architecture. Specificity is defined by direct hydrogen bonds between all streptose functional groups and base edges that line the inner walls of the cylindrical binding pocket. By contrast, the majority of intermolecular interactions involve contacts to backbone phosphates in the published structure of streptomycin bound to the 16S rRNA.

Introduction

Aminoglycoside antibiotics are known to target complex RNA structural domains such as the bacterial ribosome, spliceosome, and catalytic RNAs [1–7]. Much effort has been devoted toward understanding how the polycationic charged amines on the aminoglycosides are able to discriminate between alternate RNA folding topologies using chemical [8, 9], computational [10], NMR spectroscopic [11, 12], and crystallographic [13–15] approaches. These studies have highlighted a set of principles associated with molecular recognition, including the concept of electrostatic complementarity dictated by anion distribution within electronegative RNA binding pockets, directed intermolecular hydrogen-bonding interactions, encapsulation of the ligand within the RNA binding pocket, and the role of divalent cations and hydration in extending shape complementarity by filling cavities.

Much of the structural effort has focused on aminoglycosides bound either to modular constructs of the ribosomal RNA decoding site in solution [16–18] and in crystal [14, 15] or to crystallographic structures of complexes formed at the ribosomal subunit level [13]. Nevertheless, there are other cellular and viral RNAs that can be targeted by aminoglycosides, most likely using recognition elements that are distinct from those used to target the ribosome.

We have adopted an approach based on the in vitro selection of small RNA molecules (30 to 60 nucleotides) which bind antibiotics with high selectivity and affinity [19]. Our previous research on the solution structures of aminoglycoside antibiotics tobramycin [20] and neomycin [21] bound to their respective RNA aptamers [22, 23] established that shape and electrostatic complementarity as well as hydrogen bonding and encapsulation account for exclusive cognate ligand recognition [24].

We now turn our attention to an RNA aptamer that binds streptomycin with high specificity and affinity [25]. The aminocyclitol antibiotic streptomycin (Figure 1B) was the second antibiotic after penicillin to have a dramatic impact on medical practice and treatment. Streptomycin interacts with the central domain of 16S ribosomal RNA [1] and also inhibits group I intron splicing [3]. By contrast, bluensomycin (Figure 1B, inset), a streptomycin analog where the para-positioned guanidino group is replaced by a carbamido group, does not inhibit splicing [3]. A recent 3.0 Å crystal structure of streptomycin bound to the small ribosomal subunit has defined the intermolecular contacts between the antibiotic and multiple RNA domains of the 16S RNA [13].

A modular streptomycin binding RNA aptamer has been identified by in vitro selection in the Renee Schroeder laboratory [25]. The RNA aptamer was selected from a starting RNA library using dihydrostreptomycin-coupled sepharose affinity chromatography. A counterselection was undertaken against bluensomycin so that the RNA aptamer favors streptomycin over bluensomycin by four orders of magnitude. Streptomycin-RNA aptamer complex formation occurs with micromolar affinity and, strikingly, has an absolute requirement for divalent cations as an essential cofactor for the interaction. To establish the principles of molecular recognition, we have determined the crystallographic structure of the streptomycin binding RNA aptamer complex at 2.9 Å resolution.

Results

Crystallization of Complex

The minimal streptomycin binding 46-mer RNA aptamer identified by Wallace and Schroeder [25] contained two asymmetric internal loops separated by a stem containing three Watson-Crick pairs. One of the flanking stem segments was capped by a hairpin loop whose residues were not involved in antibiotic recognition. The 40-mer RNA aptamer construct for crystallization trials lacks the hairpin loop and is composed of two strands with single complementary base overhangs at their 5′ ends (Figure 1A). The residues within both asymmetric internal loops of the RNA aptamer which are critical for complex formation were identified in [25] and are highlighted in cyan and gold. Crystals of the streptomycin-RNA aptamer complex (1.5:1.0 ratio) grew under both 30 mM Mg (Mg-form) and 25 mM Mg/12.5 mM Ba (Ba-derivative) conditions. Sodium salt was added to the crystallization buffer in order to slow down the crystal

*Correspondence: pateld@mskcc.org
[1]These authors contributed equally to this work.

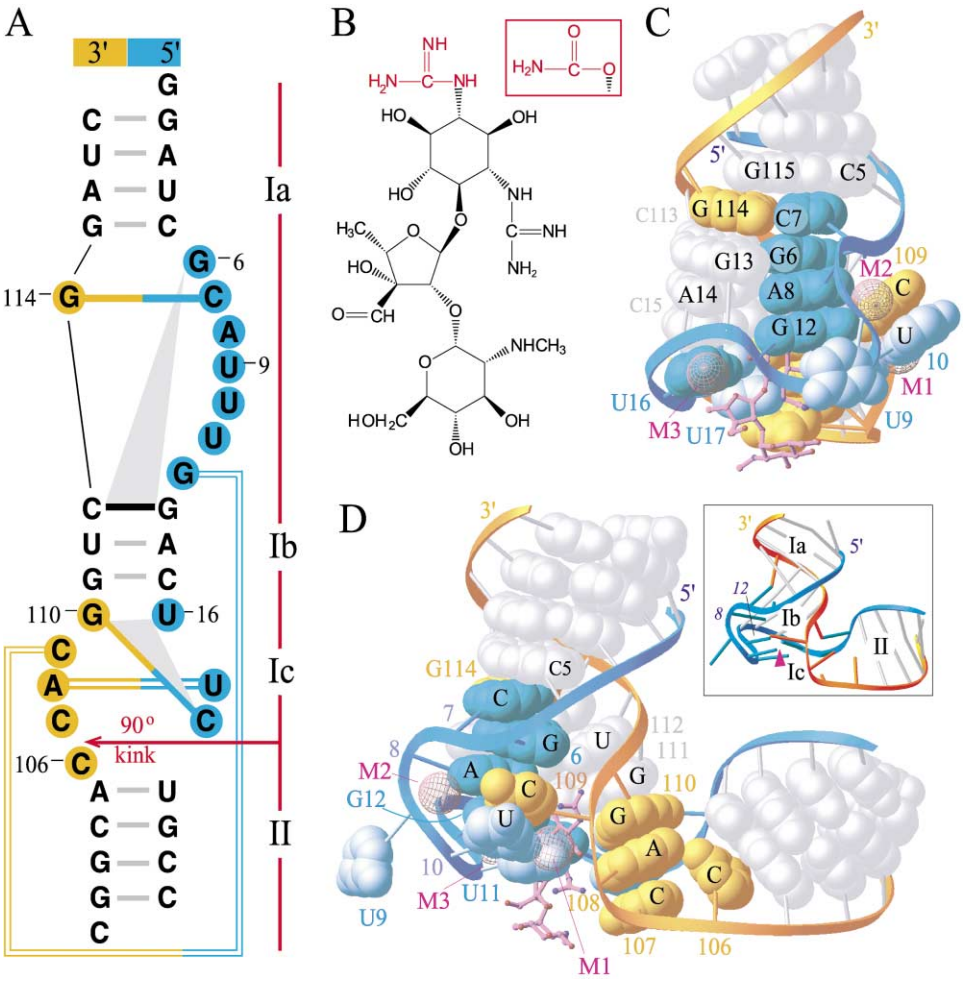

Figure 1. Two Views of the Streptomycin-RNA Aptamer Complex

(A) Secondary structure of the streptomycin RNA aptamer construct and pairing alignments derived from X-ray structure. The residues within both asymmetric internal loops that are critical for complex formation are shown in cyan and gold for 5′ and 3′ RNA strands, respectively. The two loops are separated by a three base pair stem segment (stem Ib). Canonical Watson-Crick pairs are shown as solid lines, noncanonical pairs are shown as open lines, and the base triples are shown as gray triangles. The residues of 5′ and 3′ strands are numbered 1–22 and 101–118, respectively.

(B) Formula of streptomycin. The para-substituted guanidino group is replaced by a carbamido group (inset) on proceeding from streptomycin to bluensomycin.

(C and D) Two perpendicular views of the streptomycin-RNA aptamer structure (Mg form). RNA backbone, ribose rings, and base atoms are shown as ribbons, sticks, and van der Waals spheres, respectively. Streptomycin molecule is shown in ball-and-stick mode (atoms: C, magenta; N, blue; O, red; bonds, magenta). The coordinated cations M1, M2, and M3 are shown as large magenta spheres. Selected residues are labeled. The inset in (D) shows the RNA fold with stems Ia, Ib, and Ic being almost colinear, whereas stem II is perpendicular to stem I.

growth from hours to weeks. Details of the crystallization buffers, crystal quality, and data collection are outlined in the Experimental Procedures section. The crystals belong to the tetragonal space group and contain one aptamer complex in the asymmetric unit (Table 1).

Structure Determination

The structure of the streptomycin-RNA aptamer complex was solved by the single wavelength anomalous diffraction (SAD) technique. Three Ba cations found per RNA aptamer complex were used for phasing. An electron density map derived from SAD phases is depicted in Figure 2A. Phasing power and figure of merit are listed in Table 1. The existence of the 9 base pair double-helical A-RNA-like segment formed by the Watson-Crick pairs of the Ia and II stems of the symmetry-related molecules that interact via their sticky ends in the crystal significantly facilitated the interpretation of the experimental map and allowed the building of 90% of the structure (residues 1–7, 13–22, 101–108, and 110–122). Residues 8–12 and 109 of the upper and lower loops, respectively, were inserted one by one during further model refinement, and the subsequent examination of σ-weighted Fourier synthesis map was calculated with the combined SAD and model phases. The structure refinement was completed with a final R factor of 22.2% (R_{free} = 28.2%). The first application of the SAD technique on Ba ions was performed using a single site and known

Table 1. Crystal Data, X-Ray Data Collection, and Statistics

	Ba Derivative		Mg Form
Crystal		Tetragonal	
Space Group		*I* 4	
Unit cell a = b (Å), c (Å)	83.10, 49.47		82.63, 49.15
Asymmetric unit			
Volume (Å^3)	43,000		41,950
RNA, drug residues		40 bases, 1 streptomycin	
Data collection (F > 0)			
X-ray source, detector		Rigaku RU-H3R, R-axis-IV++ Image Plate	
Wavelength (Å)		1.5418	
Resolution (Å)		30–2.9 (3.0–2.9)	
Mosaicity (°)	0.6		0.7
Unique reflections	3813 (373)		3774 (371)
Completeness (%)	99.8 (99.5)		99.9 (100)
Redundancy	9.6		5.1
R_{merge}[a]	0.064 (0.38)		0.057 (0.32)
Structure solution	SAD		Mol. replacement
Anomalous scatters	3 Ba^{+2} ions		—
$\Delta F/F$[b]	0.06		—
Phasing power[c]	1.46		—
Figure of merit prior to and after DM	0.30/0.89		—
Structure refinement			
R factor, R_{free}[d] (%)	22.2 (34.1), 28.2 (37.5)		20.8 (30.0), 25.5 (35.9)
No. of solvent molecules[e]	3 Ba^{+2}, 2 Na^+		1 Mg^{+2}, 2 Na^+, 6 H_2O
Rms bonds (Å)/angles (°)	0.012/1.78		0.010/1.75

The values in parentheses refer to data in the last resolution shell.
[a] $R_{merge} = \Sigma_{hkl}\Sigma_i|I(hkl)_i - <I(hkl)>|/\Sigma_{hkl}\Sigma_i<I(hkl)_i>$ over *i* observations of a reflection hkl. R_{merge} was calculated without averaging the intensities for Fridel pairs for Ba derivative.
[b] $\Delta F/F$ = sqrt(<||F(+)| − |F(−)||**2>)/sqrt(1/2(<|F(+)|>**2+<|F(−)|>**2)).
[c] Phasing power = sqrt<Fh^2>/sqrt<var_loc^2>, where Fh is the heavy structure factor amplitude, and var_loc is the residual lack of closure error.
[d] $R_{factor} = \Sigma_{hkl}|F(hkl)_{obs} - F(hkl)_{calc}|/\Sigma_{hkl}F(hkl)_{obs}$; R_{free} is the same calculated with 5% data withheld from refinement.
[e] Two ions have irregular coordination spheres, don't exhibit anomalous effects, and could be assigned to either Na or Mg cations at 2.9 Å resolution; they are listed as Na in the deposited coordinate files.

DNA decamer crystal structure that diffracted to relatively high resoluton of 1.7 Å [26]. Here we demonstrate that Ba cations could be successfully introduced into crystals of a 40 base RNA aptamer as well as establish the applicability of the SAD technique on Ba cations for novel RNA structure determination using X-ray data at 2.9 Å.

The Mg-form structure at 2.9 Å resolution was determined by the molecular replacement method using the refined structure of the Ba derivative. The structure was refined to a final R factor of 20.8% (R_{free} = 25.5%). The selected refinement parameters are listed in Table 1. The final σ-weighted 2Fobs-Fcalc Fourier map calculated for the Mg form around the bound streptomycin molecule is shown in Figure 2B. The loop residues 8–12 and 109 are shown in stereo in Figure 2C. The structures of the Mg form and Ba derivative exhibit similar architectures with an average root-mean-square (rms) deviation of 0.6 Å. The parallel examination of the electron density maps in Mg-form and Ba-derivative crystals and the anomalous difference map calculations performed with the combined SAD and refined model phases of the Ba derivative allowed identification of the cation binding sites and those which can be unique for Ba cations. Further structure analysis and representation were performed on the Mg form of the streptomycin-RNA complex.

Structure of Complex

Two perpendicular views of the Mg-form of the streptomycin-RNA aptamer complex are shown in Figures 1C and 1D. The color scheme for the RNA bases is the same as in Figure 1A, with the asymmetric internal loops residues of the two strands colored cyan and gold, respectively. The inset in Figure 1D shows the RNA fold in ribbon-stick representation, with stems Ia, Ib, and Ic being almost colinear, whereas stem II is perpendicular to stem I. A pronounced kink occurs at the C106-C107 step as a consequence of C18•G110 pair formation. The 5′ backbone of the upper loop forms a characteristic S-turn and brings together the conserved residues of the upper and lower loops to form the streptomycin binding pocket. The binding pocket is located at the bottom of the stem I and occupies the deep groove spanning five steps (A14•U112, C15•G111, C18•G110, U17•A108, C107) capped by the residues A8 through G12 (upper loop) and the residues U16 and C109 (lower loop).

Cation Binding Sites

We have identified three cation binding sites in the Mg-form crystals. Three ions, labeled M1 to M3, are shown as magenta spheres (Figures 1C, 1D, and 2C) and directly coordinate the RNA and stabilize the unusual con-

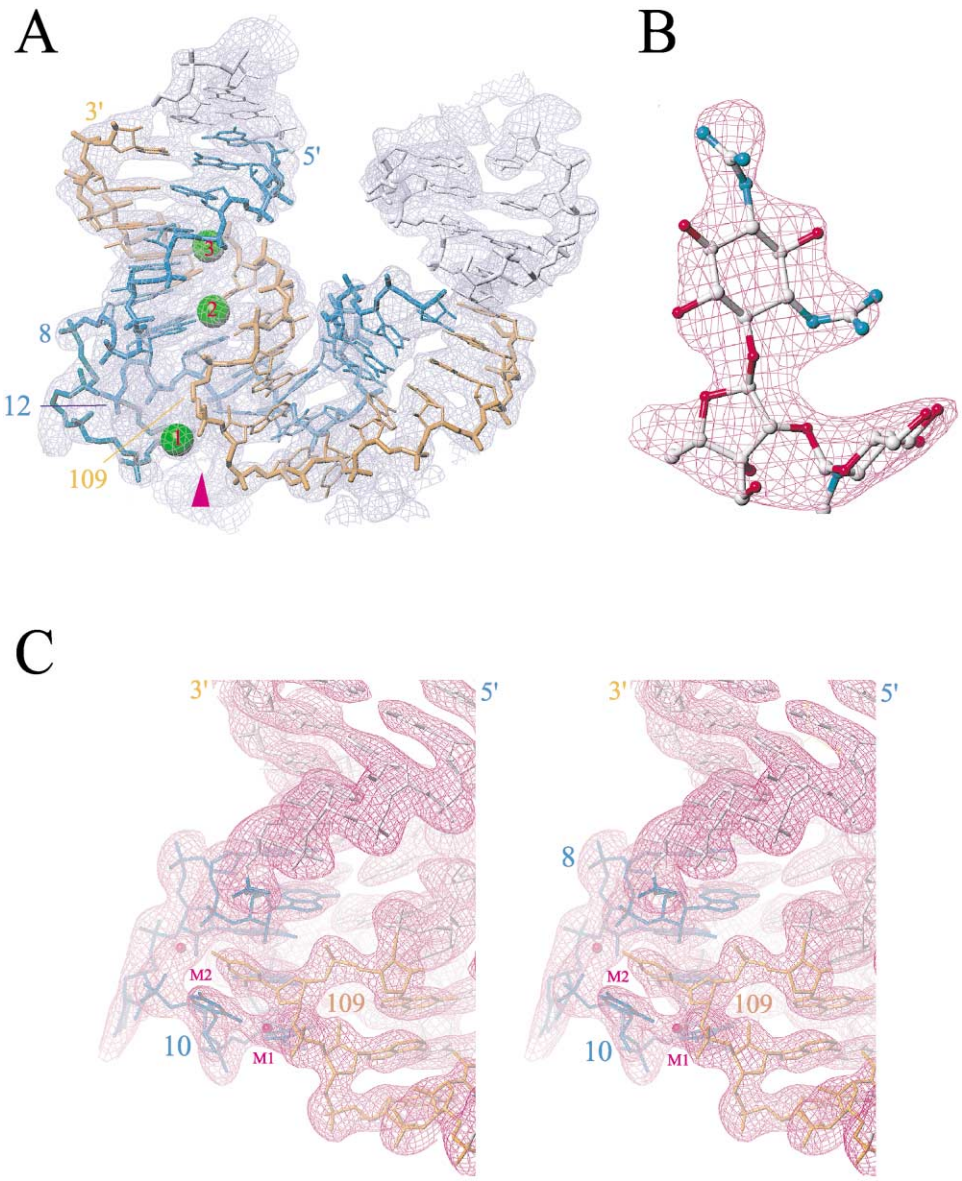

Figure 2. The Electron Density Maps

(A) Quality of the experimental electron density map calculated with the SAD phases derived from three Ba cation sites. The Ba cations are shown as green spheres. The electron density is contoured at 1σ. The view is into the deep groove of stem Ib. The coloring scheme is as follows: 5′ strand residues 1–22, cyan; 3′ strand residues 101–118, gold. Symmetry-related molecules attached via their sticky ends are shown in gray. The magenta arrow identifies the streptomycin binding pocket. Only the phosphate group connected by O5′-C5-C4′-C3′-O3 bonds is shown for the loop residues 8–12 and 109.

(B) The final σ-weighted 2Fobs-Fcalc Fourier map contoured at 1σ for bound streptomycin in the complex (Mg form). The bound streptomycin is shown in ball-and-stick mode (atoms: C, gray; N, cyan; O, red).

(C) The same map around the selected RNA bases (Mg form) shown in stereo. The loop residues 8–12 and 109 are labeled. The coordinated cations M1 and M2 are labeled and shown as small magenta spheres.

formation of the 5′ strand. The details of ion coordination are shown in Figure 3. A Mg cation (labeled M1) has well-defined octahedral coordination with ion-ligand distances close to 2.0 Å and bridges together the residues U10, U11, and C109 (Figures 2C and 3C). In the Ba derivative, this site is occupied by a Ba cation (labeled 1 in Figure 2A), which gives the strongest peak in the anomalous Patterson map. Two additional cations, M2 and M3, that are found in the Mg form have irregular coordination spheres that could be assigned to either Na or Mg ions at 2.9 Å resolution. The ion M2 stabilizes the close contact between the phosphate groups of the residues C7 and U10 (Figures 3A and 3C). The ion M3 resides between the three phosphate groups of residues G12, A14, and C15 and directly coordinates to the keto-oxygen O4 of the residue U16 (Figure 3). In the Ba derivative, no anomalous signal was found at either M2 or M3 sites. By contrast, the peaks were present at both M2

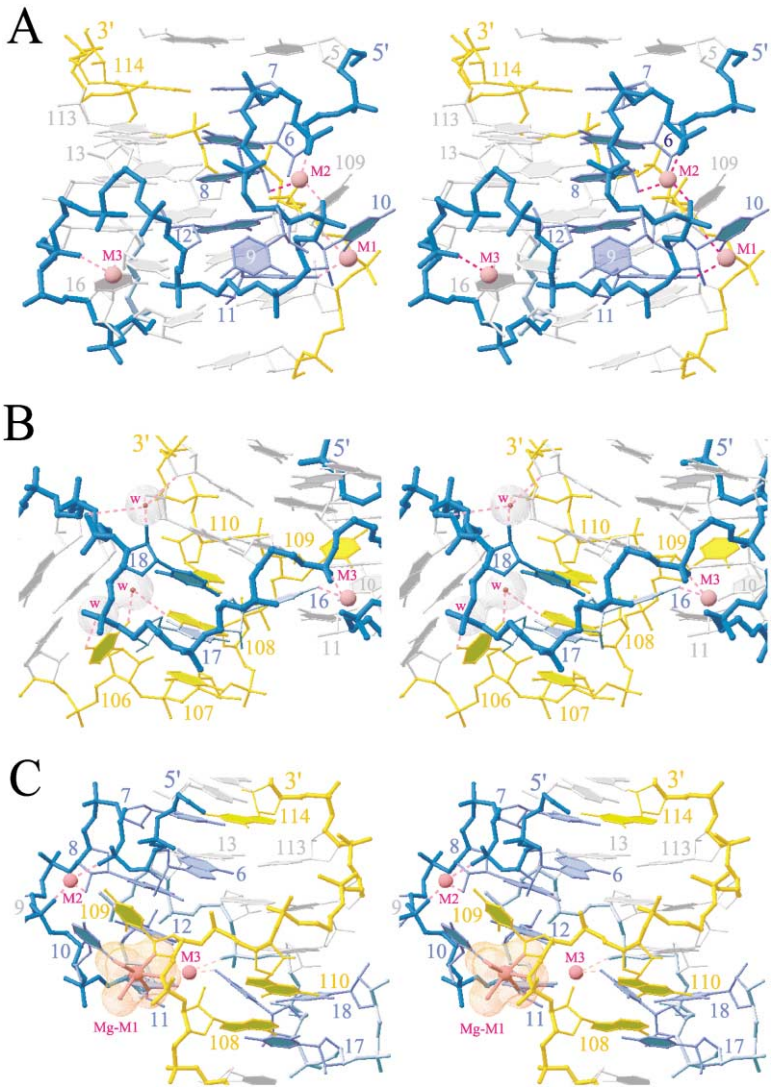

Figure 3. Stereo Views of Three Segments of the RNA Aptamer Fold in the Complex

(A) Folding of the upper asymmetric internal loop in the complex. The emphasis is on the cyan-colored strand and highlights the S-shaped turns that encompass residues G6 to G12. Three metal cations, M1 to M3, that directly coordinate to RNA and stabilize the unusual conformation of the 5′ strand are shown as magenta spheres; the direct cation-RNA contacts are indicated by magenta dashed lines. M2 coordinates to O2′ atom of A8 and O2P atoms of C7 and U10; the average distance is 2.5 Å. M3 coordinates to O2P atom of C15 and O4 atom of U16; the average distance is 2 Å.

(B) Folding of the lower asymmetric internal loop in the complex. The emphasis on the cyan-colored 5′ strand highlights residues U16 to G18, while the emphasis on the gold-colored 3′ strand highlights residues C106 to G110. The formation of the Watson-Crick C18•G110 base pair is critical for the folding of the lower loop. Three bound water molecules (labeled w) form several hydrogen bonds to the bases of both perpendicular stems, with distances shorter than 3.5 Å shown as magenta dashed lines.

(C) The interlocking of upper (G6 to G13 in cyan; G114 in gold) and lower (U16 to G18 in cyan; C107 to G110 in gold) asymmetric internal loops is stabilized by Mg cation M1. This Mg cation, shown as a magenta sphere bonded to its ligands, has well-defined octahedral coordination with ion-ligand distances of 1.9–2.1 Å. The coordination sphere consists of two keto oxygens, O2 and O4, of the residues U10 and U11, respectively, two sugar O4′ and O5′ oxygens of residues C109, and two water molecules.

and M3 sites in σ-weighted Fourier synthesis and difference maps calculated for the refined Ba-derivative structure. Thus, these sites are not favored for Ba binding, but Na or Mg cations still could occupy them even at the reduced concentration used in the crystallization of Ba derivative (see details in Experimental Procedures).

Upper Asymmetric Internal Loop

A stereo view outlining the topology of the upper asymmetric internal loop (residues 6 to 12 in cyan and residue 114 in gold) and flanking stem segments is shown in Figure 3A. The backbone chain that spans residues G6 through G12 forms an S-turn with A8 and U10/U11 being at the first and second curves, respectively. This S-turn is further bracketed by two adjacent trinucleotide turns centered at the residues G6 and G13. The residues G6 and G13 together with C113 from the partner strand form a G6•G13•C113 base triple (Figure 4B) which is sandwiched between the Watson-Crick C7•G114 loop pair (Figure 4A) and the Watson-Crick A14•U112 stem pair. The stacked C7•G114 pair and G6•G13•C113 base triple bridge stems Ia and Ib to form a continuous helical segment. The residues U9 and U10 are bulged out and exposed to the solvent. Residue U9 is involved in a crystal packing interaction with residue C107 of the symmetry-related molecule (not shown). Residue U10 is stacked on the bulged-out residue C109 of the lower loop (Figure 4D). Due to the sharp turn, the residue G12 has the sugar in the 3′-5′ polarity (opposite to its neighbors) and stacks between the base of A8 and sugar of U11. The bases of residues A8, U11, and G12 face the streptomycin binding pocket.

The segment C5-G6-C7-A8 exhibits an unusual 5-7-6-8 stacking interaction (Figure 4C). Thus, C7 is inserted between extended C5 and G6, while G6 is inserted between extended C7 and A8. Note the sugar-base hydrogen bonds between C7(O2′) and G6(N2) (Figure 4A) and between G6(O2′) and A8(N7) (Figure 4B) which help to stabilize the reversed 7-6-8 stacking (Figure 4C). In the Ba derivative, Ba cation directly coordinates to N7 and O6 atoms of the residue G6 (Figure 4C) and gives the second peak in the anomalous map. The Ba cation is surrounded by the dotted van der Waals surface and is

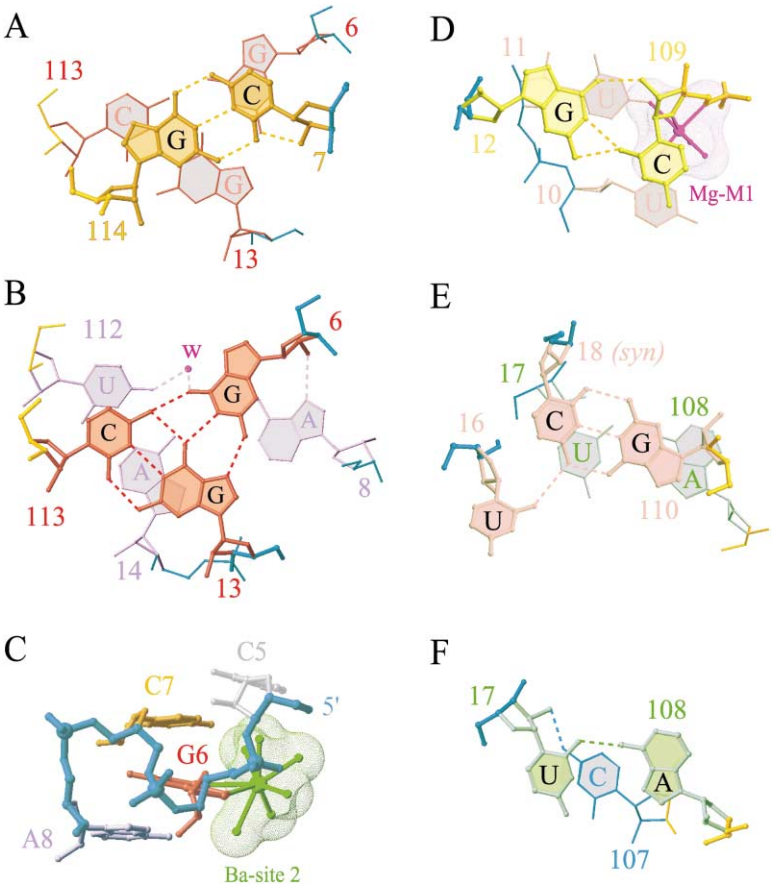

Figure 4. Formation of Canonical and Non-canonical Base Pairs and Base Triples

(A) Watson-Crick C7•G114 base pair (in gold) and its stacking with the G6•G13•C113 base triple (in red). The hydrogen bonds (2.6–3.3 Å) are shown as dashed lines.

(B) The G6•G13•C113 base triple (in red) and its stacking with the planar alignment of A8 and the A14•U112 base pair (in violet). Note water molecule (w) bridging the residues G6 and U112.

(C) The reversed 5-7-6-8 stacking adopted by the C5-G6-C7-A8 segment of the upper asymmetric internal loop. Note the sugar-base hydrogen bonds between C7(O2′) and G6(N2) (A) and between G6(O2′) and A8(N7) (B), which help to stabilize the reversed 7-6-8 stacking. In the Ba derivative, Ba cation directly coordinates to N7 and O6 atoms of the residue G6 and gives the second peak in the anomalous Patterson map. Ba cation is surrounded by the dotted van der Waals surface, which is shown as a green sphere bonded to N7, O6 atoms and six water molecules.

(D) The reversed G12•C109 noncanonical pair (in yellow) and its stacking with the cation-coordinated U10-U11 step (in pink).

(E) The U16•C18•G110 base triple (in pink) and its stacking with adjacent reversed U17•A108 noncanonical pair (in green). C18 adopts the *syn* alignment.

(F) The reversed U17•A108 noncanonical pair (in green) and its stacking with C107 (in cyan).

shown as a green sphere bonded to N7, O6 atoms, and six water molecules in Figure 4C. This binding site is unique for Ba cation, since no ordered peak was found in the Mg-form crystal.

Lower Asymmetric Internal Loop

A stereo view outlining the topology of the lower asymmetric internal loop (residues 16 to 18 in cyan and residues 106 to 110 in gold) is shown in Figure 3B. The formation of the C18•G110 base pair is critical for the folding of the lower loop. The 5′-trinucleotide U16 to C18 backbone of the loop makes a U-turn resulting in a 3′-5′ sugar polarity for residue C18 and its inverted stacking on the residue U17. Residue C18 adopts a *syn*-conformation and pairs with residue G110 via three Watson-Crick H-bonds (Figure 4E). Residues C18 and U16 are located approximately in the same plane and form one weak H bond between C18(N4) and U16(O2) atoms, resulting in a U16•C18•G110 triple with ion M3 stabilizing the position of U16 (Figure 3A). Residue C109 is bulged out and pairs with residue G12 (Figure 4D), while adjacent residue A108 pairs with residue U17 (Figure 4F). The 90° kink occurs at the bottom of the lower loop at the C106-C107 step. While residue C107 is hydrogen bonded (base-sugar zipper alignment) to the hydroxyl group of the residue U17 (Figure 4F), completing stem Ic, the residue C106 with two coordinated water molecules is stacked on the residues of stem II. Zippered-up stem Ic, which consists of three stacked alignments (G12•C109 pair [Figure 4D], U16•C18•G110 triple [Figure 4E], and U17•A108 pair [Figure 4F]), stacks, in turn, on stem Ib. Water molecules, shown as van der Waals gray dotted spheres (Figure 3B), form several hydrogen bonds to the bases of both perpendicular stems. Distances shorter than 3.5 Å are shown as magenta dashed lines. Additional water molecules reside between the sugars of residues G11, C18, and U112 and stabilize the close interactions between 5′- and 3′-backbones at the kink point.

Cation-Mediated Juxtaposition of Upper and Lower Asymmetric Internal Loops

A stereo view highlighting the interactions between the upper and lower asymmetric internal loops (residues 7 to 18 in cyan and residues 107 to 114 in gold) is shown in Figure 3C. The interlocking of upper and lower loops is stabilized by Mg ion M1. Residue C109 escapes from the stem Ic to form a sandwich with the sugar of residue G6 and the base of residue U10 of the upper loop. Residue C109 forms a noncanonical base pair with the residue G12 (Figure 4D). The octahedral coordination of Mg ion is well defined and consists of six oxygen atoms: two keto oxygens, O2 and O4, of the residues U10 and U11, respectively, two sugar O4′ and O5′ oxygens of residues C109, and two water molecules (Figure 3C). The direct RNA-ion contacts range from 1.9 to 2.1 Å and are shown as solid magenta bonds.

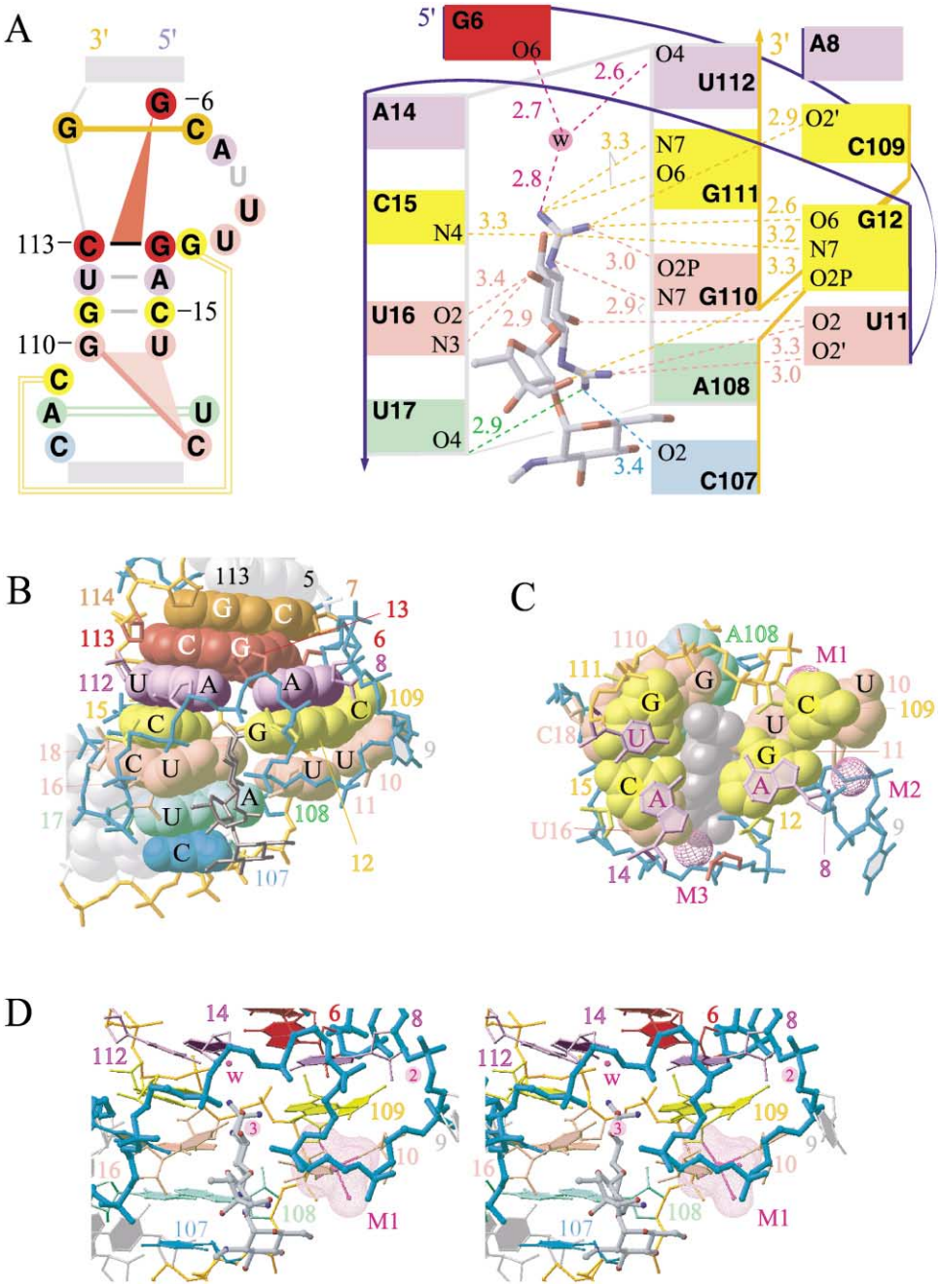

Figure 5. The Streptomycin Binding RNA Pocket

(A) RNA coloring scheme and hydrogen-bonding alignment between streptomycin and RNA residues that line the binding pocket. The bases assembled within the same plane are defined by one color. Seven sequential layers are shown in orange, red, violet, yellow, pink, green, and cyan. The streptomycin molecule is shown in a ball-and-stick mode: C, gray; N, blue; O, red. Hydrogen bond lengths between nonhydrogen atoms are listed.

(B and C) Two perpendicular views of the stacked arrays of base planes forming the binding pocket. The sugar-phosphate backbones are shown in ball-and-stick mode; the bases are shown as van der Waals spheres. The bound streptomycin is shown in gray (ball-and-stick mode in [B]; van der Waals spheres in [C]). The planar alignment of A8 and the A14•U112 base pair is shown in the ball and stick mode in (C). The coordinated metal cations are shown as large magenta spheres in (C); they are omitted in (B). The streptomycin streptose ring is buried within the cavity that is formed by the RNA deep groove of three (C15•G111, C18•G110•U11, U17•A108) steps (B, left) and capped by residues A8, G12•C109, and U10 (B, right). The base triple G6•G13•C113 (red) is located above the binding pocket and ties up stem Ib with the upper loop residues.

(D) Stereo view of the streptomycin binding pocket.

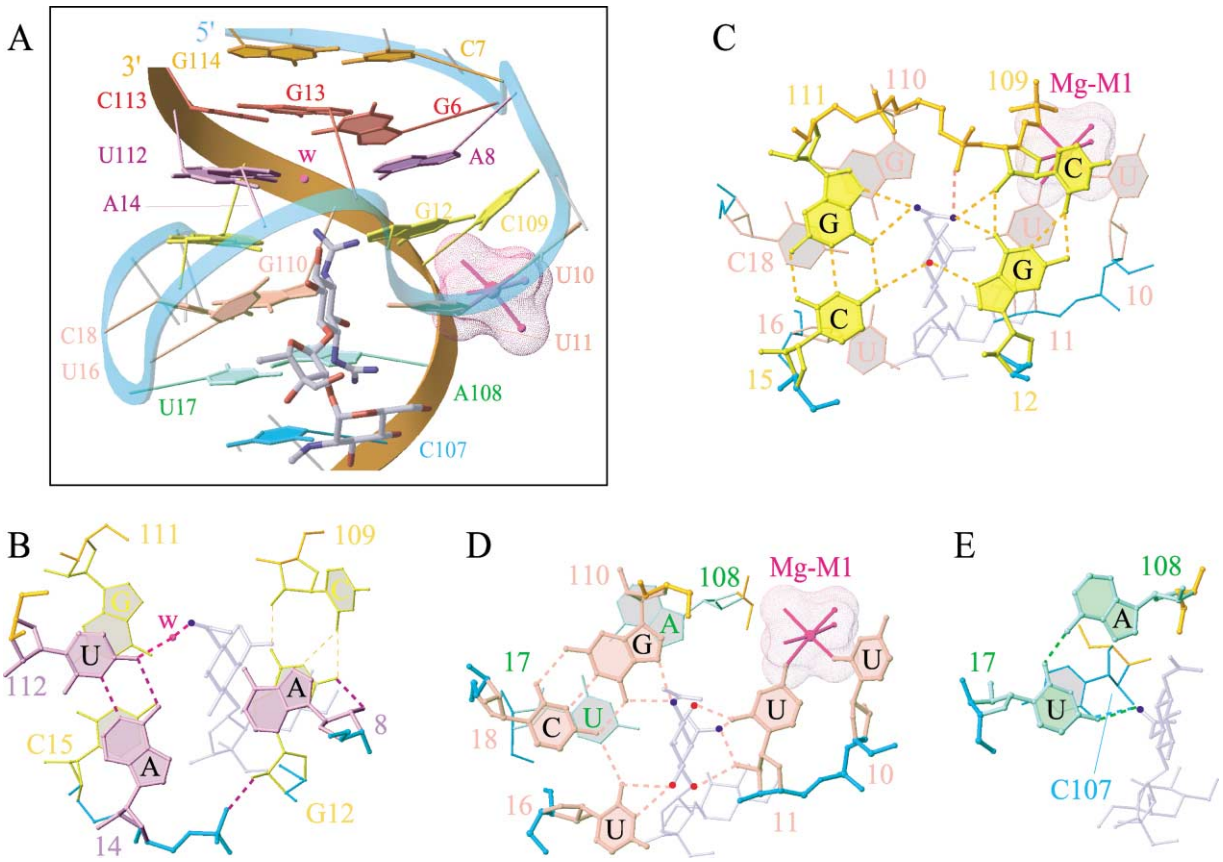

Figure 6. RNA Base Arrays Lining the Streptomycin Binding Pocket

(A) Ribbons representation of the binding pocket. The RNA bases and streptomycin molecule are shown in a ball-and-stick mode. The RNA bases are colored according to the color scheme in Figure 5. The following atom type colors are applied to the drug molecule: C, gray; N, blue; O, red.

(B) The A14•U112 pair and A8 (in purple) positioned along opposing walls of the binding pocket.

(C) The C15•G111 and G12•C109 pairs (in yellow) positioned along opposing walls of the binding pocket.

(D) The U16•C18•G110 triple and Mg-coordinated U10-U11 step (in pink) positioned along opposing walls of the binding pocket.

(E) The U17•A108 pair (green) stacked with C107 that forms one wall at the bottom of the binding pocket. The bases on top are shown with thick bonds, and the hydrogen bonds are indicated with dashed lines.

Streptomycin Binding Pocket

Streptomycin inserts itself into a RNA pocket formed at the elbow of the L-shaped architecture of the complex (Figure 1D), which incorporates elements from both asymmetric internal loops. A schematic of the RNA aptamer segment involved in the recognition is shown in Figure 5A, with bases assembled within the same plane identified by individual colors. The stacked arrays of the base planes in the aptamer core are shown in Figures 5B and 5C, with the bound streptomycin (in gray) shown in the stick mode in Figure 5B and as van der Waals spheres in Figure 5C. The stereo view of the streptomycin binding pocket is shown in Figure 5D. Seven sequential layers are shown in orange, red, violet, yellow, pink, green, and cyan. The streptose ring of streptomycin is buried in the cavity whose walls are formed by residues from the upper and lower asymmetric internal loops. Within the violet layer, the opposing walls are composed of the Watson-Crick A14•U112 pair and the A8 residue (Figure 6A), while within the yellow layer the opposing walls are made up of Watson-Crick C15•G111 and noncanonical G12•C109 pairs (Figure 6B). Within the pink layer, the opposing walls are made up of the U16•C18•G110 triple and the coplanar U10-U11 step (Figure 6C), while within the green layer there is only one surface involving the noncanonical U17•A108 pair stacked over flanking C107 base (in cyan) (Figure 6D). The binding pocket is capped at the top by the G6•G13•C113 base triple (Figure 4B). The intermolecular hydrogen bonds between the two guanidino and three hydroxyl groups on the bound streptose ring and nucleoside base edges and sugar 2′-OH groups within individual layers of the binding pocket are depicted in Figures 6A–6D. The distances between nonhydrogen atoms are indicated in Figure 5A.

Discussion

Structure Determination

Several groups have devised novel strategies to overcome the phase problem in RNA crystallography [27, 28]. These include the use of halogenated pyrimidines, ions such as lanthanides and osmium tetroxide, as well as through the introduction of U1A RNA modules to

capitalize on the known structure of the U1A protein-RNA hairpin complex. More recently, the anomalous diffraction properties of Zn have been exploited to solve the phase problem in RNA crystallography [29] even though Zn is a poor substitute for Mg. We have taken an alternate approach which uses the anomalous dispersion properties of Ba, a divalent cation located within the same column of the periodic table as Mg. We have been able to crystallize and solve the structure of the streptomycin-RNA aptamer complex grown from a 25 mM Mg/12.5 mM Ba-containing solution (Ba derivative; for details see Experimental Procedures). The SAD analysis was undertaken on a data set collected on a standard Rigaku diffractometer (wavelength = 1.54 Å, E = 8.0 keV using CuKalpha radiation). Three Ba sites were located, of which one (labeled 1) exhibited full occupancy, while the other two sites (labeled 2 and 3) exhibited partial occupancy (Figure 2A). It turns out that only one Ba site (labeled 1) coincides with the Mg site (labeled M1) found in the Mg form, and two other sites are unique for Ba cation. The Ba cations penetrate within the deep groove of stem Ia and bind to the O6/N7 edges of the residue G6 (labeled 2) and the residues G114 and G115 (labeled 3). We anticipate that introduction of Ba and utilization of its anomalous properties could play a key role in crystallography of RNA and its complexes.

Global Topology of the RNA Fold and Antibiotic Binding Site

The RNA adopts an unexpected L-shaped architecture on complex formation with streptomycin. The upper and lower zippered-up asymmetric loops together with the upper and central stems form one continuous helix which is kinked by 90° relative to the lower stem (Figures 1A and 1D). Unpaired residues C106 and C107 are positioned orthogonally to each other at the kink site (Figure 1D). The cyan-labeled strand, which contains residues G6 to G12 and U16 to U18 from the upper and lower asymmetric internal loops, respectively, undergoes a series of S-shaped turns which position key residues for antibiotic recognition. The distinct conformation of this strand is stabilized by three cations. The gold-labeled strand, which contains residues G114 and C106 to G110 from the upper and lower asymmetric internal loops, respectively, adopts a more regular backbone fold, except for the sharp turn at the C106-C107 step. The streptomycin binding pocket is located at the elbow of the L-shaped architecture and accommodates the streptose ring within a cylindrical cavity formed by the walls of residues contributed by the two asymmetric internal loops.

Zippering Up the Two Asymmetric Internal Loops

The upper asymmetric internal loop zippers up such that the loop C7•G114 pair (in orange) is sandwiched between helical C5•G115 (gray, upper stem) and G13•C113 (red, central stem) pairs (Figure 5B). Loop residue G6 participates in G6•G13•C113 base triple formation and is stacked on C7. While A8 (violet) is stacked between G6 (in red) and G12 (in yellow), U9 is bulged out. The U10-U11 step (in pink) is anchored in place by a Mg cation M1 and stacks on G12 (in yellow), which is paired with C109 from the lower loop. The residues A8, U11, and G12 are directed toward the antibiotic binding pocket (Figure 5C, right).

The lower asymmetric internal loop zippers up and forms a continuous stacked helical segment with base pairs of the central stem (Figure 5B, left). Thus, the C15•G111 pair (in yellow) of the central stem stacks with the lower loop C18•G110 pair (in pink), which in turn stacks with the lower loop noncanonical U17•A108 pair (green, Figure 5B). Loop residue U16 is part of the U16•C18•G110 triple and is stacked within the extended stem I. All residues of the lower loop are involved in the formation of the antibiotic binding pocket.

Pairing Alignments within Loops

We have identified four additional pairing alignments involving loop residues in the structure of the streptomycin-RNA aptamer complex, and these are indicated in Figures 5A and 6A. One of these (C7•G114) involves residues in the upper loop, two (C18•G110 and U17•A108) involve residues in the lower loop, while G12•C109 involves residues from both loops. Both C7•G114 (Figure 4A) and C18•G110 (Figure 6D) pair through Watson-Crick alignment, while G12•C109 (Figure 6C) and U17•A108 (Figure 6E) form reversed noncanonical pairs. The Watson-Crick edge of G12 pairs with both the base and sugar 2′-OH of C109, while the Watson-Crick edge of U17 pairs with the Hoogsteen edge of A108. The noncanonical G12•C109 pair is critical since it aligns the upper (through G12) and lower (through C109) loops to generate the streptomycin binding pocket (Figure 5B).

We have identified two base triples that participate in stabilization of the extended stem I in the structure of the complex. One of the triples involves residue G6, which pairs with both bases along the major groove edge of the G13•C113 Watson-Crick pair of the central stem (Figure 4B). Such an alignment, which brings residues G6 and G13 in the same plane, is feasible as a consequence of the S-shaped topology of the 5′-backbone of the upper loop. The other triple involves residue U16, which pairs with C18 along the major groove edge of the C18•G110 Watson-Crick pair (Figures 5B and 6D). The anchoring of U16 through triple formation both orients and positions it for recognition of the bound antibiotic.

Unpaired Loop Residues

Unpaired residues from both the upper and lower asymmetric internal loops play both architectural and recognition roles in the streptomycin-RNA aptamer complex. Residues C106 and C107 of the lower loop flank the kink site, with C106 stacked on stem II, while C107 is stacked on stem I. Residues U9 and U10 of the upper loop are part of the S-turn of the cyan-containing strand, with U9 looped out of the extended helix I and U10 stacked with C109 of the lower loop. The latter stacking contributes to alignment of the upper (through U10) and lower (through C109) loops to generate the streptomycin binding pocket.

Unpaired residues A8 (Figure 6A) and U11 (Figure 6C) from the upper loop and U16 (part of the U16•G18•G110 triple) (Figure 6C) and C107 (Figure 6D) from the lower

loop are directed toward the antibiotic binding pocket and are involved in molecular recognition of the bound streptomycin.

Streptomycin Binding Pocket

A unique feature of the complex is the participation of residues originating within both asymmetric internal loops in sculpting the streptomycin binding pocket (Figure 5). The series of S-shaped turns positions U11 and G12 of the upper loop and U16 and U17 of the lower loop of the 5′ strand to interact with the bound antibiotic. Lower loop residues C107, C109, and G110 of the 3′ strand are also positioned to interact with the bound antibiotic. In addition, the major groove edge of the Watson-Crick C15•G111 pair of the central stem plays a key role in molecular recognition. A cylindrical cavity is generated by loop residues of both strands, with the antibiotic sandwiched within the walls, each of which is lined with base and base pair edges for molecular recognition. The dimensions of the cavity are such that only the nonsugar streptose ring penetrates into it and is anchored by a intermolecular hydrogen-bonding network (Figures 5 and 6). The furanose and pyranose rings are positioned outside the pocket and are less well defined than the streptose ring (Figure 2B). This fact is related to the RNA aptamer counterselection from a starting RNA library against bluensomycin that differs from streptomycin only in para-position of the streptose ring.

Molecular Recognition

The streptose ring recognizes the RNA stacked bases layer by layer using all of the NH_2, NH, and OH atoms (Figure 6). The majority of the intermolecular hydrogen bonds are of the direct type, except for one at the top of the pocket which involves a bridging water molecule.

The para-substituted guanidinium functionality of the streptose ring penetrates most deeply into the binding pocket and is anchored in place through hydrogen bonds involving both its NH_2 groups and its NH group. It is approximately positioned in the plane (in yellow) formed by the opposingly positioned G12•G109 and C15•G111 pairs and hydrogen bonds with the major groove edge of two guanines, G12 and G111, and the sugar 2′-OH of the cytosine C109 (Figures 5A and 6C). In addition, the para-substituted guanidinium is positioned facing the phosphate group of G110 with at least one good H bond being formed to its O2P atom (Figures 5A and 6C). In total, there are seven electronegative atoms (N7, O6/O4 O2P) in the 2.8-4.1 Å sphere around the NH_2 atoms suggestive of a positively charged para-substituted guanidinium group. This guanidinium $(NH_2)_2^+$-C-NH group is replaced by a carbamido NH_2-CO-O group in bluensomycin. Hence, it is not surprising that the para-substituted guanidinium group plays a central role in molecular recognition, given that the RNA aptamer for streptomycin was identified following counterselection against bluensomycin.

The ortho-substituted guanidinium group is positioned at the entrance to the cavity and is also anchored through intermolecular hydrogen bonds involving both its NH_2 groups and residue C107 of the gold-colored 3′ strand and residues U11 and U17 associated with the S-turns of the cyan-colored 5′ strand (Figure 5A). Here, a mixture of hydrogen bonds to base edges (U11, U17, and C107) and 2′-OH groups (U11) define the alignment within the pocket (Figures 6D and 6E). Thus, the two guanidinium groups span opposite ends of the binding pocket and anchor the streptose ring within it.

All three hydroxyl groups of the streptose ring form intermolecular hydrogen bonds with base/base pair edges lining the antibiotic binding pocket associated with the U11-G12 and C15-U16 steps on the cyan-colored 5′ strand (Figure 5A).

Chemical Probing Data

Chemical probing experiments using dimethyl sulfate had previously identified adenosines and cytosines within the upper and lower asymmetric internal loops which are protected from modification on streptomycin-RNA aptamer complex formation [25]. These include C7, A8, and C18 on the 5′ strand and C106, A108, and C109 on the 3′ strand (Figure 5A). These chemical probing results are consistent with our X-ray structure of the streptomycin-RNA aptamer complex. Thus, C7 forms a Watson-Crick pair with G114 (Figure 4A), C18 forms a Watson-Crick pair with G110 (Figure 6D), A108 forms a reversed noncanonical pair with U17 (Figure 6E), and C109 forms a reversed noncanonical pair with G12 (Figure 6C). A8 is stacked into the extended stem I and directed toward but not paired with the A14•U12 pair (Figure 6B). C106 is located at the site of the 90° kink in the L-shaped structure, stacks over the terminal A•U base pair of stem II in one direction, and is buttressed by an orthogonally oriented C107 in the opposite direction (Figure 1D). In addition, asymmetric internal loop residues C107 and C109 form intermolecular hydrogen bonds with the bound streptomycin in our X-ray structure of the complex (Figures 6E and 6C, respectively).

Chemical probing experiments with kethoxal were unable to identify guanines within the upper and lower asymmetric internal loops which are protected from modification on streptomycin-RNA aptamer complex formation [25]. We find these conclusions to be inconsistent with our X-ray structure of the streptomycin-RNA aptamer complex, since our structure predicts that asymmetric internal loop guanines G114 (which participates in C7•G114 Watson-Crick pair, Figure 4A), G6 (which participates in the G6•G13•C113 triple, Figure 4B), G12 (which participates in the reversed G12•C109 noncanonical pair, Figure 6C), and G110 (which participates in C18•G110 Watson-Crick pair, Figure 6D) should be protected from kethoxal modification on streptomycin-RNA aptamer complex formation. In addition, asymmetric internal loop residues G12 and G110 form intermolecular hydrogen bonds with the bound streptomycin in our X-ray structure of the complex (Figures 6C and 6D).

The RNA aptamer has been shown in Pb cleavage studies to undergo a conformational change which spans both asymmetric internal loops on addition of streptomycin in Mg-containing solution [25]. We do not know the structure of the free RNA aptamer, but the asymmetric internal loops clearly participate in strepto-

mycin recognition in our X-ray structure of the streptomycin-RNA aptamer complex.

Design Principles

The X-ray structure of streptomycin bound to the small ribosomal subunit has been solved in the Ramakrishnan laboratory at 3.0 Å resolution [13]. All three rings of streptomycin are involved in recognition, with interactions spanning four different domains of 16S RNA and a lysine side chain of the S12 protein. The majority of the intermolecular contacts involve hydrogen bonds or salt bridges to backbone phosphates. These results are in striking contrast to our X-ray structure of the streptomycin-RNA aptamer complex, where only the streptose ring is embedded and involved in molecular recognition within the RNA fold, and recognition predominantly involves intermolecular hydrogen bonding to the base edges, a few 2′ hydroxyl groups, and one backbone phosphate. Thus, different recognition principles have emerged from studies of streptomycin to the small ribosomal subunit [13] and a RNA aptamer (this study).

Bluensomycin (Figure 1B, inset) differs from streptomycin (Figure 1B) in that a carbamido group has replaced the para-substituted guanidino group. Thus, two acceptors have replaced two donor moieties, and perhaps the available structure of the streptomycin binding aptamer (that discriminates against bluencomycin by four orders of magnitude) could provide insights into the minimal number of substitutions necessary to convert it into a bluensomycin binding RNA aptamer. We note that one of the NH_2 groups and the NH group of the para-substituted guanidino group of streptomycin are hydrogen bonded to acceptor atoms along the major groove edges of G111 and G110, respectively, in our structure of the complex (Figures 6C and 6D). Replacement of these two guanines by adenines at positions 110 and 111 would provide donor amino groups which can then hydrogen bond to the acceptor carbonyl and ester oxygens of the para-substituted carbamido group of bluensomycin. To maintain Watson-Crick pairing, C18•G110 would have to be replaced by U18•A110, and C15•G11 would have to be replaced by U15•A111. Thus, our prediction would be that four targeted substitutions encompassing two base pairs is likely to be sufficient to switch a streptomycin binding RNA aptamer to a bluensomycin binding RNA aptamer counterpart. It is conceivable that additional changes may be required to accommodate the anticipated electrostatic perturbation, since the charged guanidino group in streptomycin has a neutral carbamido counterpart in bluensomycin.

Comparison with Other RNA Aptamer Complexes

Arginine binding and citrulline binding RNA aptamers contain two asymmetric internal loops separated by a two base pair stem [30–32]. The secondary folds for the arginine and citrulline binding RNA aptamers have elements in common with the streptomycin binding RNA aptamer. The structures of the arginine/citrulline-RNA aptamer complexes have been solved by homonuclear NMR spectroscopy [33]. The binding cavities in these complexes are distinct from that observed in our structure of the streptomycin-RNA aptamer complex. Thus, the majority of the binding pocket residues come from the larger of the two asymmetric internal loops, and the bound arginine/citrulline are positioned over a G•G platform and intermolecularly hydrogen bonded by recognition residues that are directed at various angles to this platform.

Another comparison can be made with an RNA aptamer that targets theophylline and discriminates against closely related caffeine [34]. The secondary fold of this RNA aptamer also contains two asymmetric internal loops separated by a two base pair stem. The structure of the theophylline-RNA aptamer complex has been solved by heteronuclear NMR spectroscopy [35]. The binding pocket is generated by interlocking of residues from the two internal loops and involves a sandwich of three base triples, with the planar theophylline being part of the central triple. Additional features involve base zippers, adenosine platforms, S-turns involving reversed sugars, and 1-3-2 stacking motifs. Despite S-turns, reversed sugars, and 1-3-2 stacking motifs being common elements in both the theophylline-RNA aptamer [35] and streptomycin-RNA aptamer (this study) complexes, the binding pocket architectures are very distinct for the planar and neutral theophylline and the nonplanar charged streptomycin.

Thus, it appears that RNA folds containing two asymmetric internal loops separated by a short stem can adopt a range of ligand-dependent RNA architectures. This is not surprising since the RNA folds around the bound ligand, and ligand shape, charge, and hydrogen-bonding potential determines the topology and functional groups that line the RNA binding pocket.

Significance

Noncoding RNAs are believed to play critical roles in RNA processing and modification, messenger RNA stability and translation, and transcriptional regulation [36]. These RNAs can adopt novel folded topologies, and the resulting scaffolds can be targeted by small molecules ranging from natural antibiotics to combinatorially synthesized ligands [8–10, 37–41]. Our approach has been to structurally characterize RNA aptamer complexes selected for their high affinity and specificity to systematically increase our understanding of shape and electrostatic complementarity, intermolecular stacking, and directional hydrogen bonding as well as elucidate what principles contribute to discriminatory molecular recognition.

Our X-ray structure of the streptomycin-RNA aptamer complex defines the architecture of the streptose binding RNA pocket sculpted through interaction between a pair of asymmetric internal loops and highlights the role of directed intermolecular hydrogen bonds involving primarily base edges to discriminate between streptomycin and bluensomycin. The extensive use of S-turns, involving 1-3-2-4 stacking motifs, formation of both canonical and noncanonical base pairs and triples on complex formation, together with encapsulation of the streptose ring within a cylindrical cavity lined with stacked arrays of bases defines novel principles and patterns associated with both RNA ar-

chitecture and ligand recognition. The location and partial identity of bound cations stabilizing packed elements of the central core of the complex together with our exploitation of the anomalous diffraction properties of divalent Ba cations to solve the crystallographic phase problem has added a new approach to the crystallographic structure determination of RNA and its complexes.

We anticipate that recognition principles which have emerged from our previous NMR solution structural studies of RNA aptamer complexes with tobramycin [20] and neomycin [21] and the current crystallographic structural study of the streptomycin-RNA aptamer complex could provide insights into the design of aminoglycoside antibiotics that could potentially target natural RNAs and modulate their function.

Experimental Procedures

Synthesis, Crystallization, and Data Collection

Purified 22-mer and 18-mer RNA strands r(GGAUCGCAUUUGGA CUUCUGCC) and r(CGGCACCACGGUCGGAUC) were purchased from Dharmacon Research. The RNA strands were dissolved in water, mixed at equimolar ratio, heated (95°C for 2 min), and snap cooled on ice. Then, divalent salt was added to this RNA sample, and the solution incubated at 37°C for 10 min (5 mM divalent salt, 5 mM Na-cacodylate buffer, pH 6.5). At this point, streptomycin in aqueous solution (Sigma) was added to a drug/RNA ratio of 1.5:1, and the solution was incubated for another 10 min. We have used magnesium, barium, manganese, strontium, cobalt, copper, and zinc chlorides as divalent salts. Only crystals grown in the presence of magnesium and barium chloride were suitable for X-ray experiments. Complex formation was monitored by recording one-dimensional imino proton NMR spectra in H_2O solution of the free RNA, RNA-Mg, and streptomycin-RNA-Mg complex. Single crystals of the streptomycin-RNA complex were grown at 20°C using the hanging drop vapor diffusion technique. To obtain Mg-form crystals, the droplet (4μl) containing the RNA-streptomycin complex (0.18 mM) in 13 mM MES buffer (pH 5.6), 30 mM $MgCl_2$, 100 mM NaCl, 5% MPD was equilibrated against a 0.6 ml reservoir. The reservoir solution was 20% MPD, 50 mM MES buffer (pH 5.6), 100 mM $MgCl_2$, 70 mM NaCl. To obtain Ba-derivative crystals, the droplet (3 μl) containing the RNA-streptomycin complex (0.24 mM) in 17 mM MES buffer (pH 5.6), 12.5 mM $BaCl_2$, 25 mM $MgCl_2$, 65 mM NaCl, 6% MPD was equilibrated against 0.6 ml reservoir. The reservoir solution was 17.5% MPD, 50 mM MES buffer (pH 5.6), 25 mM $BaCl_2$, 75 mM $MgCl_2$, 65 mM NaCl. Tetragonal crystals of size 0.05 × 0.05 × 0.5 mm (Mg form) and 0.1 × 0.1 × 1.0 mm (Ba derivative) grew in about a month's time. The crystals were briefly soaked in 20% MPD and shock frozen under liquid nitrogen. Single crystal X-ray data sets were collected using in-house X-ray source (360° oscillation range, 0.25° oscillation width, 10 min exposure time, 75 mm crystal-to-detector distance). X-ray data were integrated and scaled with DENZO/SCALEPACK suite [42], and selected crystal data and data collection parameters are summarized in Table 1. The crystals were checked using synchrotron radiation, and no improvement in the diffraction pattern was found.

X-Ray Structure Solution and Refinement

The Ba-derivative structure was determined by the SAD technique. Heavy atom search, Patterson map, electron density map calculations, and SAD phasing were performed with the program CNS [43], and maps were displayed with the program TURBO-FRODO [44]. The heavy atom search was applied to anomalous-difference Patterson maps calculated at 4.0 Å, and one well-defined Ba site was located. SAD phasing was then performed using all data to 2.9 Å resolution. In order to find more Ba sites, the above SAD phases were used in combination with the anomalous difference structure factors to compute anomalous-difference Fourier and double-difference maps. Two additional Ba sites were found; the relative occupancy of the three Ba sites labeled 1, 2, and 3 are 1, 0.5, and 0.33, respectively.

To solve the Mg-form structure, we have used molecular replacement method using Ba-derivative structure as a starting model and the program AmoRe [45]. Rigid-body and initial positional refinement for both Ba-derivative and Mg-form crystal structures were carried out with the program CNS. The TLS and bulk solvent parameters, restrained temperature factor, and final positional refinement were completed with the program REFMAC [46]. The selected refinement parameters are listed in Table 1. Examples of the final σ-weighted 2Fobs-Fcalc Fourier maps are shown in Figures 2B and 2C for Mg form.

Acknowledgments

This work was supported by funding under GM54777 from the NIH to D.J.P. The crystals were checked at the BioCARS beam line on Sector 14 at the Advanced Photon Source, Argonne National Laboratory, U.S. Department of Energy, Office of Basic Energy Sciences, contract number W-31-109-Eng-38.

Received: December 19, 2002
Revised: January 28, 2003
Accepted: January 29, 2003

References

1. Moazed, D., and Noller, H.F. (1987). Interaction of antibiotics with functional sites in 16S ribosomal RNA. Nature *327*, 389–394.
2. Recht, M.I., Douthwaite, S., Dahlquist, K.D., and Puglisi, J.D. (1999). Effect of mutations in the A-site of 16S rRNA on aminoglycoside antibiotic-ribosome interaction. J. Mol. Biol. *286*, 33–43.
3. von Ahsen, U., and Schroeder, R. (1991). Streptomycin inhibits splicing of group I introns by competition with the guanosine substrate. Nucleic Acids Res. *19*, 2261–2265.
4. Rogers, J., Chang, A.H., von Ahsen, U., Schroeder, R., and Davies, J. (1996). Inhibition of the self-cleaving reaction of the human hepatitis delta virus ribozyme by antibiotics. J. Mol. Biol. *259*, 916–925.
5. Stage, T.K., Hertel, K.J., and Uhlenbeck, O.C. (1995). Inhibition of hammerhead ribozyme by neomycin. RNA *1*, 95–101.
6. Hermann, T., and Westhof, E. (1998). Aminoglycoside binding to the hammerhead ribozyme: a general model for the interaction of cationic antibiotics with RNA. J. Mol. Biol. *276*, 903–912.
7. Tor, Y., Hermann, T., and Westhof, E. (1998). Deciphering RNA recognition: aminoglycoside binding to the hammerhead ribozyme. Chem. Biol. *5*, R277–R283.
8. Tor, Y. (1999). RNA and the small molecule world. Angew. Chem. Int. Ed. Engl.*38*, 1579–1582.
9. Sucheck, S.J., and Wong, C.-H. (2000). RNA as a target for small molecules. Curr. Opin. Chem. Biol. *4*, 678–686.
10. Hermann, T., and Westhof, E. (1998). RNA as a drug target: chemical, modeling and evolutionary tools. Curr. Opin. Biotechnol. *9*, 66–73.
11. Fourmy, D., Yoshizawa, S., and Puglisi, J.D. (2001). Structural basis of aminoglycoside action. In RNA-Binding Antibiotics, R. Schroeder and M. Wallis, eds. (Georgetown, TX: Landes Bioscience), pp. 11–23.
12. Jiang, L., and Patel, D.J. (2000). Encapsulation of tobramycin and neomycin B within similar RNA aptamer binding pockets. In RNA-Binding Antibiotics, R. Schroeder and M. Wallis, eds. (Georgetown, TX: Landes Bioscience), pp. 112–121.
13. Carter, A.P., Clemons, W.M., Brodersen, D.E., Morgan-Warren, R.J., Wimberly, B.T., and Ramakrishnan, V. (2000). Functional insights from the structure of the 30S ribosomal subunit and its interactions with antibiotics. Nature *407*, 340–348.
14. Vicens, Q., and Westhof, E. (2001). Crystal structure of paromomycin docked into the eubacterial ribosomal decoding A site. Structure *9*, 647–658.
15. Vicens, Q., and Westhof, E. (2002). Crystal structure of the complex between the aminoglycoside tobramycin and an oligonu-

cleotide containing the ribosomal decoding site. Chem. Biol. *9*, 747–755.
16. Fourmy, D., Recht, M.J., Blanchard, S.C., and Puglisi, J.D. (1996). Structure of the A site of E. coli 16S rRNA complexed with an aminoglycoside antibiotic. Science *274*, 1367–1371.
17. Yoshizawa, S., Fourmy, D., and Puglisi, J.D. (1998). Structural origins of gentamicin antibiotic action. EMBO J. *17*, 6437–6448.
18. Lynch, S.R., and Puglisi, J.D. (2001). Structural origins of aminoglycoside specificity for prokaryotic ribosomes. J. Mol. Biol. *306*, 1037–1058.
19. Schroeder, R.E., and Wallis, M.G. (2001). RNA-Binding Antibiotics. (Georgetown, TX: Landes Bioscience).
20. Jiang, L., and Patel, D.J. (1998). Solution structure of the tobramycin-RNA aptamer complex. Nat. Struct. Biol. *5*, 769–774.
21. Jiang, L., Majumdar, A., Hu, W., Jaishree, T.J., Xu, W., and Patel, D.J. (1999). Saccharide-RNA recognition in a complex formed between neomycin B and an RNA aptamer. Structure *7*, 817–827.
22. Wang, Y., and Rando, R.R. (1995). Specific binding of aminoglycoside antibiotics to RNA. Chem. Biol. *2*, 281–290.
23. Wallis, M.G., von Ahsen, U., Schroeder, R., and Famulok, M. (1995). A novel RNA structure for neomycin recognition. Chem. Biol. *2*, 543–552.
24. Hermann, T., and Westhof, E. (2001). New strategies for docking cationic drugs to RNA targets. In RNA-Binding Antibiotics, R. Schroeder and M. Wallis, eds. (Georgetown, TX: Landes Bioscience), pp. 146–156.
25. Wallace, S.T., and Schroeder, R. (1998). *In vitro* selection and characterization of streptomycin-binding RNAs: Recognition discrimination between antibiotics. RNA *4*, 112–123.
26. Tereshko, V., Wilds, C.J., Minasov, G., Prakash, T.P., Maier, M.A., Howard, A., Wawrzak, Z., Manoharan, M., and Egli, M. (2001). Detection of alkali metal ions in DNA crystals using state-of-the-art X-ray diffraction experiments. Nucleic Acids Res. *29*, 1208–1215.
27. Golden, B.L. (2000). Heavy atom derivatives of RNA. Methods Enzymol. *317*, 124–132.
28. Cate, J.A., and Doudna, J.A. (2000). Solving large RNA structures by x-ray crystallography. Methods Enzymol. *317*, 169–180.
29. Ennifar, E., Walter, P., and Dumas, P. (2002). An efficient method for solving RNA structures: MAD phasing by replacing magnesium with zinc. Acta Crystallogr. *D57*, 330–332.
30. Famulok, M. (1994). Molecular recognition of amino acids by RNA aptamers: an L-citrulline binding RNA motif and its evolution into an L-arginine binder. J. Am. Chem. Soc. *116*, 1698–1706.
31. Burgstaller, P., Kochoyan, M., and Famulok, M. (1995). Structural probing and damage selection of citrulline- and arginine-specific RNA aptamers identify base positions required for binding. Nucleic Acids Res. *23*, 4769–4776.
32. Geiger, A., Burgstaller, P., von der Eltz, H., Roeder, A., and Famulok, M. (1996). RNA aptamers that bind L-arginine with sub-micromolar dissociation constants and high enantioselectivity. Nucleic Acids Res. *24*, 1029–1036.
33. Yang, Y., Kochoyan, M., Burgstaller, P., Westhof, E., and Famulok, M. (1996). Structural basis of ligand discrimination by two related RNA aptamers resolved by NMR spectroscopy. Science *272*, 1343–1347.
34. Jenison, R.D., Gill, S.C., Pardi, A., and Polisky, B. (1994). High-resolution molecular discrimination by RNA. Science *263*, 1425–1429.
35. Zimmermann, G.R., Jenison, R.D., Wick, C.L., Simorre, J.P., and Pardi, A. (1997). Interlocking structural motifs mediate molecular discrimination by a theophylline-binding RNA aptamer. Nat. Struct. Biol. *6*, 644–649.
36. Storz, S. (2002). An expanding universe of noncoding RNAs. Science *296*, 1260–1263.
37. Patel, D.J. (1997). Structural analysis of nucleic acid aptamers. Curr. Opin. Chem. Biol. *1*, 32–46.
38. Afshar, M., Prescott, C.D., and Varani, G. (1999). Structure-based and combinatorial search for new RNA-binding drugs. Curr. Opin. Biotechnol. *10*, 59–63.
39. Hermann, T. (2000). Strategies for the design of drugs targeting RNA and RNA-protein complexes. Angew. Chemie Int. Ed. Engl. *39*, 1890–1905.
40. Hermann, T., and Patel, D.J. (2000). Adaptive recognition by nucleic acid aptamers. Science *287*, 820–825.
41. Gallego, J., and Varani, G. (2001). Targeting RNA with small-molecule drugs: Therapeutic promise and chemical challenges. Acc. Chem. Res. *34*, 836–843.
42. Otwinowski, Z., and Minor, W. (1997). Processing of X-ray diffraction data collected in oscillation mode. Methods Enzymol. *276*, 307–326.
43. Brünger, A.T. (1998). Crystallography & NMR System (CNS), Version 0.5. Yale University, New Haven, CT.
44. Cambillau, C., and Roussel, A. (1997). Turbo Frodo, Version OpenGL.1. Université Aix-Marseille II, Marseille, France.
45. Navaza, J. (1994). AMoRe: an automated package for molecular replacement. Acta Crystallogr. A *50*, 157–163.
46. Murshudov, G.N., Vagin, A.A., and Dodson, E.J. (1997). Refinement of macromolecular structures by the maximum-likelihood method. Acta Crystallogr. D *53*, 240–255.

Accession Numbers

Coordinates and structure factors have been deposited in the Protein Data Bank under ID codes 1NTA and 1NTB for Ba-derivative and Mg-form crystals, respectively.